EFFECTS OF SWAY AND ROLL EXCITATIONS ON SLOSHING LOADS IN A KC-1 MEMBRANE LNG TANK

Se-yeol An[1]
Hyeon-won Jeong[1]
Ohyoung Kim[2]
W. Jaewoo Shim[1,*]

[1] Department of Chemical Engineering, Dankook University, Gyeonggi-do, 16890, South Korea

[2] School of Polymer Science and Engineering, Dankook University, Gyeonggi-do, 16890, South Korea

* Corresponding author: *wjshim@dankook.ac.kr (W. Jaewoo Shim)*

ABSTRACT

This study investigates the effects of sway and roll excitations on sloshing liquid loads in a tank, using Ansys Fluent software. The model considered in the study is a 1:50 scaled membrane-type tank, based on a KC-1 membrane LNG tank designed by Korea Gas Corporation (KOGAS). The volume of fluid (VOF) method is used to track the free surface inside the tank, and the standard k-ε model is applied to express the turbulent flow of the liquid. To explore the motion of the tank under excitation, a user-defined function (UDF) and a dynamic mesh technique are employed to control the external forces exerted on the tank through its motion. The results, in the form of time series data on the sloshing pressures in the tank under pure sway, roll, and coupled sway-roll, are analysed, with specific ranges for the excitation amplitudes and frequencies. We show that variations in excitation frequency and amplitude significantly influence the sloshing loads. Sloshing loads are found to intensify when the excitation frequency matches the tank's primary natural frequency, $1.0\ \omega'_1$. Furthermore, with coupled sway-roll excitations, the sloshing loads are weakened when the sway and roll are in-phase and are intensified when these are out-of-phase. Fast Fourier transform analysis provides insights into the frequency domain, showing that the dominant frequency is 0.88 Hz and it is approximately equal to the tank's primary natural frequency, $1.0\ \omega'_1$.

Keywords: KC-1 membrane LNG tank; Sloshing; Sway; Roll; Coupled sway-roll; Fast Fourier transform (FFT)

INTRODUCTION

The term 'sloshing' refers to unrestrained movements of the free surface of a liquid in a container, and occurs when a partially filled tank is exposed to external perturbations, which cause the free surface of the liquid to oscillate [1]. In the case of small perturbations, sloshing can be approximated as a linear superposition of different wave components [2]. However, it is important to note that sloshing flow represents a complex fluid motion. Under certain conditions, the pressure exerted on the inner walls of the tank that are in contact with the liquid can increase dramatically; this is because the unrestrained free surface tends to undergo significant excursions for even small movements of the

tank [1]. Consequently, in severe cases, the loads generated by sloshing can lead to structural damage to the tank's inner walls. These issues are related to ensuring the safety of waterway transportation of liquefied natural gas (LNG) in LNG tankers. To address these concerns, it is important to predict the sloshing flow of a liquid loaded in a tank and the resulting pressure variations. Accurate predictions and an understanding of sloshing behaviour can help in devising measures to mitigate potential structural damage and enhance the safety of LNG transportation.

The motion of a tank floating on the sea has six degrees of freedom (6DOF), with external forces exerted on the tank that can include a single DOF, such as surge, sway, heave, pitch, roll, or yaw as well as multiple coupled DOFs [3]. As a result,

many studies have been conducted to investigate sloshing within tanks subjected to multiple coupled excitations [2–5]. Chen and Wu [3] conducted a study of fluid sloshing in three-dimensional tanks filled to an arbitrary depth under various excitation frequencies and motion with multiple DOFs. They demonstrated that instability of sloshing occurs when the excitation frequency of the heave motion is twice as large as the fundamental natural frequency under coupled surge-sway-heave excitations. Hou et al. [2] studied liquid sloshing in a two-dimensional tank under single and multiple coupled external excitations, such as coupled sway-roll and coupled sway-roll-heave excitations. In their research, they showed that sloshing loads are intensified when the tank experiences multiple coupled excitations and that match the first order natural frequency of the tank. Wu et al. [4] conducted experiments to investigate the impact loads from liquid sloshing at low liquid loading rates under coupled roll-pitch excitations. They observed that when the excitation frequencies for roll and pitch are between 0.98 f_1 and 1.113 f_1, where f_1 represents the first-order natural frequency of a sloshing liquid in a rectangular tank, a roof-bursting phenomenon by the liquid occurred. In addition, they noted that the maximum impact pressure was observed at 1.09 f_1.

In summary, several studies have been conducted on sloshing in tanks under various liquid filling levels and ship motions. However, limited attention has been given to investigating sloshing phenomena under the influence of coupled sway-roll excitations, which represent one of the most extreme instances of sloshing-induced structural damage within the context of the 6DOF motion of a tank [5]. The largest sloshing loads occur in the range 0.1 ≤ h/H ≤ 0.5 for the liquid filling height [5]. Hence, this study investigates sloshing in a tank filled to 50% with water under pure sway, pure roll, and coupled sway-roll excitations, to gain insights into the behaviour of the liquid and to understand the potential impacts on the structural integrity of the tank under these specific conditions.

The model considered in the study is a 1:50 scaled membrane-type tank based on the design of a 48,280 m³ KC-1 membrane LNG tank designed by Korea Gas Corporation (KOGAS) [6]. To investigate the sloshing loads, the variations in the excitation frequency and amplitude are considered in order to observe the time-dependent sloshing pressure variations over a wide range of sway, roll, and coupled sway-roll excitations, using the Ansys Fluent computational fluid dynamics (CFD) software. MATLAB software is also used to perform a fast Fourier transform (FFT) analysis of the time series results for the sloshing pressures under coupled sway-roll excitations, to provide a quantitative analysis in the frequency domain.

COMPUTATIONAL MODELING

COMPUTATIONAL MODEL

In a sloshing analysis, the free surface of a liquid exhibits nonlinearity as the external forces increase, and one challenging aspect of sloshing analysis is the accurate tracking of the flow of this nonlinear free surface. To address this issue, Hirt and Nichols [7] introduced the volume of fluid (VOF) method, which represents the volume occupied by the liquid in each computational cell as a discrete function. This method provides a solution for effectively tracking the nonlinear free surface waves. Since its introduction, the VOF method has been widely used to track the free surface in sloshing analyses, and it is also adopted in the present study, using Ansys Fluent software. Eq. (1) gives the function that expresses the volume fraction of liquid occupying a cell.

$$\alpha(x, y, z) = \begin{cases} 0 \\ 0 \sim 1 \\ 1 \end{cases} \tag{1}$$

When the value of α is zero, this represents an empty state with no liquid in the cell, while values of α between zero and one represent a free surface that includes both liquid and gas. When the value of α is one, this indicates that only liquid is present in the cell. Fig. 1 shows the volume fractions of liquid in each of the cells based on the values of α.

Fig. 1. An example of the distribution of α values in cells [8]

GOVERNING EQUATIONS

In this study, a conventional numerical approach is employed to calculate the sloshing phenomenon of liquid in a tank. It is assumed that the fluid flow is incompressible, and the turbulent flow in the sloshing phenomenon is represented by the Reynolds-averaged Navier-Stokes (RANS) equation. The Reynolds stresses and the turbulent flow field in the RANS are calculated based on the standard k-ε model. The volume

fraction for the two phases, liquid and gas, is calculated using the volume fraction equation in Eq. (2):

$$\frac{1}{\rho_q}\left[\frac{\partial}{\partial t}(\alpha_q \rho_q) + \nabla \cdot (\alpha_q \rho_q \bar{u}_q) = S_{\alpha_q} + \sum_{p=1}^{n}(\dot{m}_{pq} - \dot{m}_{qp})\right]$$

(2)

where the variables $\dot{m}_{pq}$ and $\dot{m}_{qp}$ represent the mass transfer from phases p to q and from phases q to p, respectively [9, 10]. S_{α_q} is the source term for phase q in a cell [9, 10]. Eq. (3) is the governing equation for the momentum, as follows:

$$\frac{\partial}{\partial t}(\rho \vec{u}) + \nabla \cdot (\rho \vec{u} \vec{u}) = -\nabla p + \nabla \cdot (\bar{\bar{\tau}}) + \rho \vec{g} + \vec{F}$$

(3)

where $\vec{u}$ denotes the velocity vector, ρ the density of the mixture, p the static pressure, and $\bar{\bar{\tau}}$ the stress tensor [11, 12]. $\rho \vec{g}$ and $\vec{F}$ represent the gravitational body force and external body force, respectively [11, 12]. The stress tensor, $\bar{\bar{\tau}}$, can be expressed as:

$$\bar{\bar{\tau}} = \mu(\nabla \vec{u} + \nabla \vec{u}^T)$$

(4)

where μ is the dynamic viscosity [11, 12].

EXCITATION FORCES

The tank can experience external perturbations including sway and roll excitations. Sway excitation induces a linear transverse (lateral or side-to-side) motion along the tank's transverse axis, whereas roll excitation induces a tilting rotation of the tank about its longitudinal axis, with the centre of the bottom of the tank acting as the centre of the coordinate system. If the sway and roll excitations are periodic, they can be represented in the form of sinusoidal waves, as shown below.

$$X = X_0 sin(\omega t)$$

(5)

$$\theta = \theta_0 sin(\omega t)$$

(6)

Eq. (5) is the mathematical expression for the sway excitation, while Eq. (6) is the mathematical expression for the roll excitation. Here, X and θ represent the lateral displacement and the rotational displacement, respectively. X_0 represents the amplitude of the lateral displacement, θ_0 represents the amplitude of the rotational displacement, and ω is the frequency of the excitations.

Fig. 2 shows the two-dimensional geometric parameters of a rectangular tank and a prismatic model tank. The rectangular tank is considered for the validation of modelling assumptions used in the computation, and the membrane-type tank with a prismatic shape is the model LNG tank used in the study.

To model the sway and roll excitations of the tank, the first natural frequency of the prismatic tank was used. The first natural frequency of the rectangular tank, ω_1, can be determined using Eq. (7), and its correlation with the first natural frequency of the prismatic tank, ω'_1, is expressed in Eq. (8) [13–15]:

$$\omega_1^2 = \frac{\pi g}{B} tanh\left(\frac{\pi h}{B}\right)$$

(7)

$$\frac{\omega'_1{}^2}{\omega_1{}^2} = 1 - \frac{\left[B_1 H_1^{-1} sinh\left(\frac{\pi H_1}{B}\right) - B_1 H_1^{-1} sin^2\left(\frac{\pi B_1}{B}\right)\right]}{\pi sinh\left(\frac{2\pi h}{B}\right)}$$

(8)

In this study, Eq'ns. (5) to (8) are used to apply external excitations to the tank, in order to induce prescribed motions according to specific formulae. To accurately simulate the motion of the tank under these excitations, a user-defined function (UDF) and a dynamic mesh technique are employed to impose the external excitation effectively.

The investigation focused on the effects of different excitations on the sloshing loads in the tank, including single excitations (pure sway and pure roll) and multiple coupled excitations 'coupled sway-roll'. In particular, the sloshing pressures in the tank are analysed when the excitation of roll
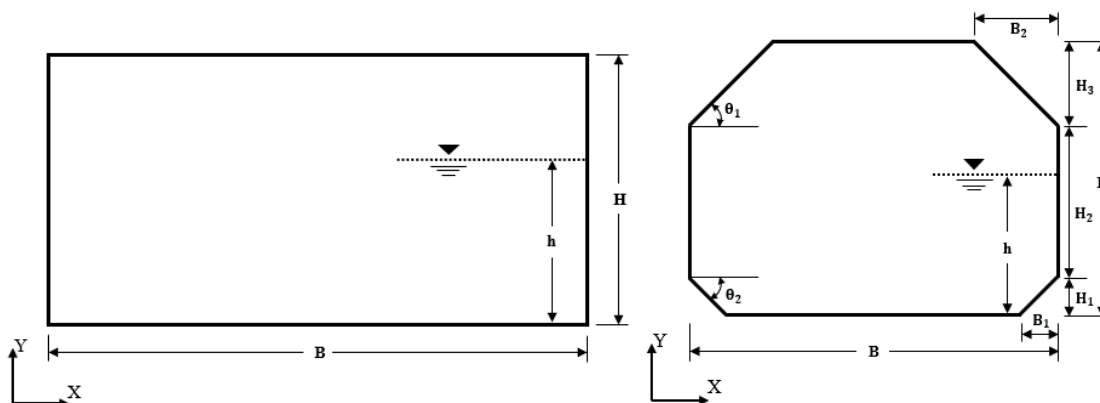

Fig. 2. Parameters for a two-dimensional rectangular tank (left) and a two-dimensional prismatic tank (right)

is coupled with the sway's in the same-phase (0°) and the opposite-phase (180°).

Fig. 3 shows the time-dependent lateral displacements of a tank subjected to a pure sway excitation having an amplitude of 0.015 m, while others are the time-dependent rotational displacements due to pure roll excitations with amplitudes of 1°, 3°, and 5° in the same-phase or the opposite-phase relative to the sway's. The frequency of the excitations was set to the first natural frequency of the tank, denoted as $1.0\ \omega_1'$.
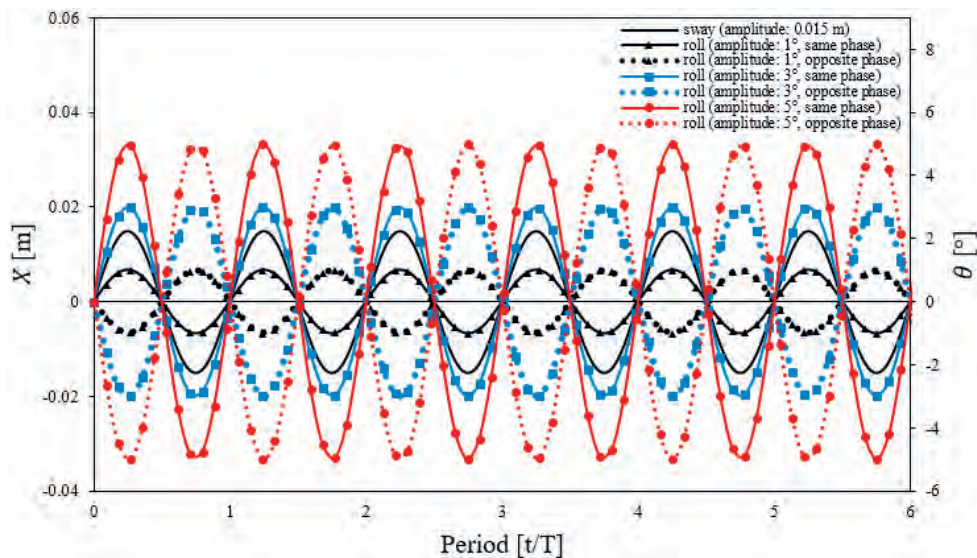

Fig. 3. Displacement of a tank due to pure sway and pure roll excitations. The roll excitation is in-phase or out-of-phase with the sway excitation

VALIDATION

To assess the validity of the modelling assumptions used for the numerical simulation, a comparison was conducted between the simulation results and experimental data obtained from a well-known prior study conducted by Hinatsu [16]. The experimental data selected for the comparison consisted of measurements of sloshing pressures in a rectangular tank under pure sway excitation. A schematic representation of the rectangular tank used in their experimental investigation is presented in Fig. 4. The tank had a base length of 1.2 m and height of 0.6 m. For the experiment, the tank was filled with water to 60% of its height from the floor, and the remaining spaces were filled with air. Subsequently, the tank was subjected to pure sway excitation characterised by an amplitude of 0.015 m and a period of 1.404 s. During the validation process, the simulation results were compared to the experimental data pertaining to the sloshing impact pressure at a specific location, denoted as P_1 at the tank wall (as indicated in Fig. 4). The primary objective of this comparison was to evaluate the degree of agreement between our simulation data and the experimental data regarding the sloshing impact pressures at the designated point.

In the numerical simulation, the fluid motion was modelled as an incompressible unsteady flow, with a no-slip condition assumed at the walls. To track the free surface, which represents the interface between the water and air, the VOF method was employed [7]. To express the turbulent flow of the liquid, the standard k-ε model was used [17]. To calculate the pressure on a computational mesh from the velocity components, the semi-implicit method for pressure-link equations (SIMPLE) algorithm was used, in which the momentum equations were coupled with an iterative procedure [18]. A compressive scheme was used to calculate the volume fraction for the interface capturing problem [19].

Fig. 4 illustrates the base case for the computational mesh used in the simulation of the rectangular tank, which was formed of a combination of triangular and rectangular grids. When excitation is applied to a tank, sloshing-induced liquid forces often impacts and shocks certain zones on the upper-left and upper-right walls of the tank, and on the roof. Furthermore, the motion of the liquid near the point of impact exhibits complex flow phenomena [20]. Thus, to accurately capture the complex flow behaviour of the liquid, smaller triangular grids (0.0025 m here in the base case) were employed near the anticipated impact zones on the walls [20, 21]. Larger rectangular grids (0.005 m in the base case) were used in the remaining regions to reduce the computational time while still maintaining reasonable accuracy. The entire mesh for the base case consisted of a total of 64,620 grid points. To assess the numerical accuracy of the results in terms of the sloshing loads in the tank with respect to the grid resolution, two cases were analysed: the base case and a coarse case of 32,132 grid points, half the number of the base case. It is important to note that in both cases, the number of grid points significantly exceeded those used in a validation process (7,200) performed by Rhee [12]. Furthermore, our study investigated the influence of the time step size on accuracy. Three time steps were compared: a base time step of 0.0005 s, a large time step of 0.001 s (twice that of the base case), and an extra-large time step of 0.002 s (twice that of the large case).
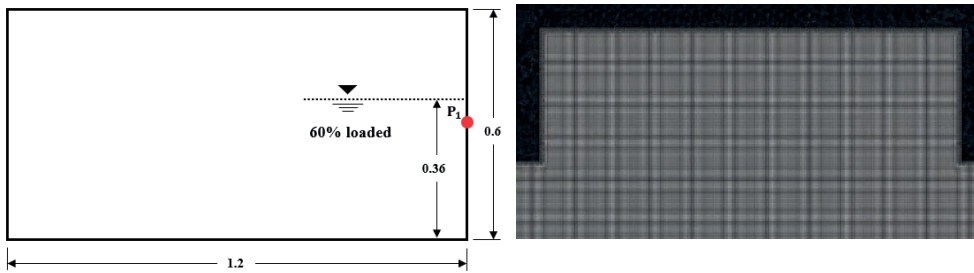
Fig. 4. Schematic of the rectangular tank used in the validation process (left) and the base case of the computational mesh for the tank (right) [Units: m]
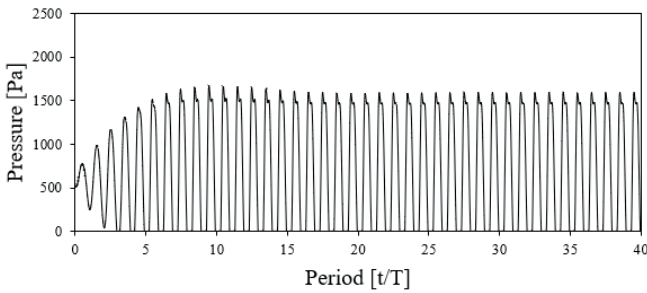

Fig. 5. Pressure history at point P_1 of the rectangular tank for the base cases of both the mesh and time step size

Tab. 1. Sensitivity of sloshing pressure at point P_1 of the rectangular tank to the number of grid points and the time step size between the 20th and 25th cycles

Mesh	Number of grid points	Average pressure [Pa]	ε [%]	$ε_{validation}$ [%]
Base	64,620	1,562.317	-	0.68
Coarse	32,132	1,577.064	0.94	1.63
Time step	**Size [s]**	**Average pressure [Pa]**	**ε [%]**	**$ε_{validation}$ [%]**
Base	0.0005	1,562.317	-	0.68
Large	0.001	1,519.703	2.73	2.06
Extra-large	0.002	1,424.312	8.83	8.21

Fig. 5 illustrates the variation in sloshing pressure at point P_1 of the rectangular tank, obtained from a simulation of the base cases for both the mesh and the time step size. The sloshing pressure initially rises, and then goes through a transient phase where it increases and subsequently decreases. After the 20th cycle, the pressure variations stabilise, and a steady-state region is reached.

Table 1 provides assessments of the simulation accuracy based on the number of grid points and the time step size. To evaluate the accuracy, the average values for the top 10% of sloshing pressure values at P_1 between the 20th and 25th cycles in the steady-state region were compared with the experimental values (comparable six cycles in steady-state region). To investigate the accuracy in terms of the number of grid points, the time step was set to the base case, whereas to investigate the accuracy in terms of the time step size, the mesh was set to the base case. The error between our simulation data and the experimental data is denoted as

$ε_{validation}$, and the error relative to the simulation values for the base cases as ε.

The results for the accuracy with respect to the number of grid points showed that ε was 0.94% for the coarse case, and the values of $ε_{validation}$ for the base and coarse case were 0.68% and 1.63%, respectively. The values for the base case, with a larger number of grid points, were more consistent with the experimental values. The results for the accuracy with a varying time step size gave values for ε of 2.73 and 8.83% for the large and extra-large cases, respectively; the values of $ε_{validation}$ for the large and extra-large cases were 2.06% and 8.21%, respectively, while $ε_{validation}$ for the base case was 0.68%. This investigation revealed that reducing the time step size led to a decrease in the error. Fig. 6 shows a graph of the variations in sloshing impact pressure at point P_1, and compares the data obtained from the simulation of the base cases for both the mesh and time step size with the experimental data. The experimental data shown in the figure were obtained by Fourier decomposition of the raw experimental data [22]. The graph shows remarkable agreement between our computed data and the experimental data, thus confirming that the assumptions used in the simulation were appropriate, and the base cases for both the mesh and time step size were therefore adopted for the simulations in the remainder of the study. These results validate the reliability and accuracy of our numerical simulation in terms of capturing the sloshing behaviour of water in a tank under the specified conditions.
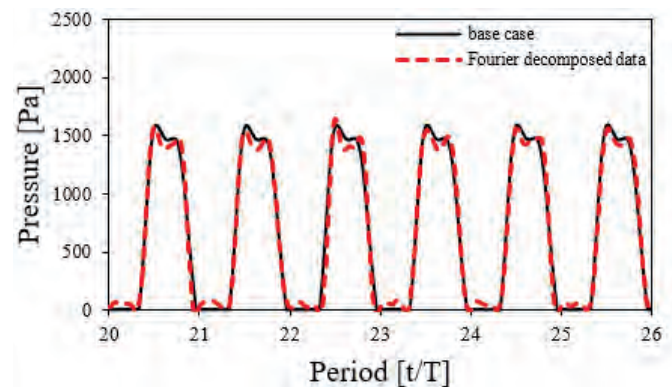

Fig. 6. Pressure history at P_1 of the rectangular tank between cycles 20 and 25: comparison of the base case simulation vs. the Fourier decomposition of experimental data [22]

RESULTS AND DISCUSSION

A simulation study was conducted using a prismatic model tank filled with 50% water, as shown in the schematic diagram in Fig. 7. The main objective of the investigation was to analyse the influence of the excitation frequency and amplitude on the sloshing pressure in the model tank under both sway and roll excitations, beyond the conditions used for the validation of the rectangular tank. To explore the effect of the excitation amplitude, three different sway amplitudes of 0.0075, 0.015, and 0.03 m were analysed. Similarly, three different roll amplitudes were examined: 1°, 3°, and 5°. In addition, the excitation was investigated at six different frequencies relative to the tank's primary natural frequency, ω'_1, with values of 0.8 ω'_1, 1.0 ω'_1, 1.2 ω'_1, 1.4 ω'_1, 1.6 ω'_1, and 1.8 ω'_1. To assess the sloshing pressure under various types of external excitation, the excitations were classified into four scenarios: pure sway, pure roll, and coupled sway-roll with both the same-phase and the opposite-phase. The study particularly focused on analysing the sloshing impact pressures at point P_1, as indicated on the tank wall in Fig. 7. In the same figure, the computational mesh used to simulate the tank is shown, to enable a visualisation of the detailed mesh structure used to capture the sloshing behaviour. In this study, we investigated the effects of sloshing on the tank under various excitation scenarios with a 50% liquid filling level, as this is a tank filling condition known for its severe sloshing-induced damage [5]. We conducted a total of 42 simulations, with 18 for pure sway, 18 for pure roll, and six for coupled sway-roll.
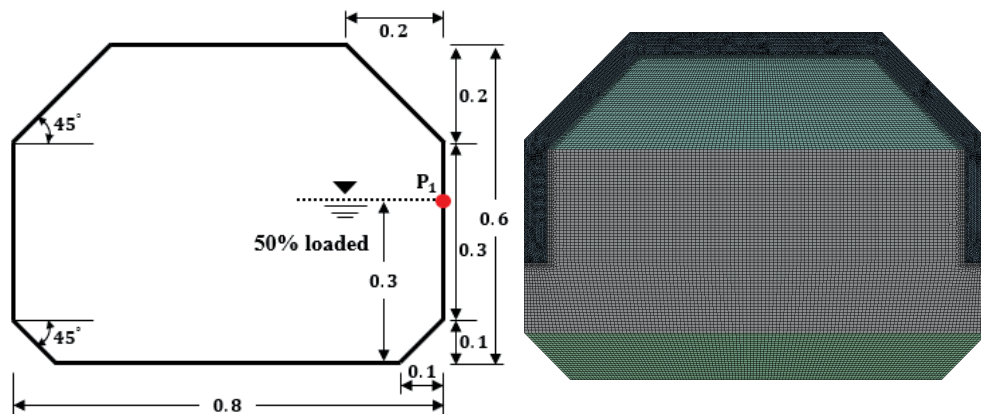
It was observed that an increase in the excitation amplitude led to an increase in the sloshing pressure. This was be attributed to the heightened excitation forces acting on the tank as the amplitude increases, which result in greater sloshing-induced forces. However, during pure rolls with frequencies of 0.8 ω'_1, 1.2 ω'_1, and 1.8 ω'_1, it was noted that the relationship between amplitude and pressure exhibited a nonlinear softening effect, leading to a reduced rate of increase in the sloshing pressure. In a study conducted by Akyildiz and Ünal [23] on sloshing pressure during pitch motion, they also found that sloshing pressure exhibited decreased sensitivity to amplitude, causing a reduction in the rate of pressure increase.

The impact of excitation frequency on sloshing pressure was also investigated. Fig. 8 shows that under pure sway excitation, the lowest pressure occurred at an excitation frequency of 1.6 ω'_1, whereas under pure roll excitation, the lowest pressure occurred at an excitation frequency of 1.4 ω'_1, under the same amplitude conditions. When the frequency of pure sway or roll was 1.0 ω'_1, the highest sloshing pressure was recorded under the same amplitude conditions. This behaviour was attributed to resonance, in which the frequency matches the tank's primary natural frequency, causing intense sloshing of the liquid. This resonance effect results in a significant increase in sloshing pressure, and in engineering design, it is important to avoid the conditions for resonance and their potential detrimental effects on the structural integrity of tanks [24, 25].

Fig. 7. Schematic of the prismatic model tank (left, actual LNG tank size: H = 29.71 m, H_1 = 4 m, H_2 = 16.507 m, H_3 = 9.203 m, B = 40.31 m, B_1 = 4 m, B_2 = 9.203 m, $\theta_1 = \theta_2$ = 45°) and the base case of the computational mesh used for the tank (right) [Units: m]

PURE SWAY AND PURE ROLL EXCITATIONS

Fig. 8 and Table 2 present the results for the sloshing pressure at point P_1 in the model tank, obtained under pure sway and pure roll excitation forces of various frequencies and amplitudes. The data include the average values of the top 10% sloshing pressures between the 16th and 21st cycles, after the transient phase.

Tab. 2. Average pressures at P_1 for the prismatic model tank under pure sway or roll excitations [Units: Pa]

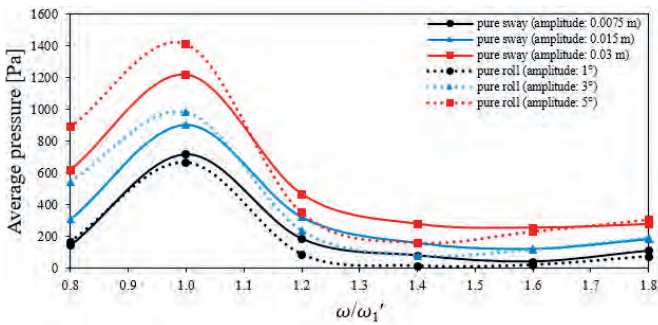| Frequency	Pure sway			Pure roll		
	Amplitude			Amplitude		
	0.0075 m	0.015 m	0.03 m	1°	3°	5°
0.8 ω'_1	141.153	309.174	618.612	165.666	546.482	886.990
1.0 ω'_1	716.198	903.424	1219.392	666.429	981.332	1409.812
1.2 ω'_1	183.924	321.814	465.267	87.447	236.756	347.834
1.4 ω'_1	79.544	160.115	277.848	13.921	79.483	159.855
1.6 ω'_1	40.974	123.624	254.184	19.642	116.830	228.883
1.8 ω'_1	109.614	184.812	276.799	73.855	191.390	303.609

Fig. 8. Average pressures at P_1 for the prismatic model tank vs. excitation frequency of pure sway and pure roll

COUPLED SWAY-ROLL EXCITATIONS

We also investigated several cases of coupled sway-roll excitations for the model tank, which were divided into two types, with the opposite-phase or the same-phase. The opposite-phase cases were Case 1 (roll amplitude: 1°), Case 2 (roll amplitude: 3°), and Case 3 (roll amplitude: 5°), while the same-phase cases were Case 4 (roll amplitude: 1°), Case 5 (roll amplitude: 3°), and Case 6 (roll amplitude: 5°). In all cases, the amplitude of the sway excitation was fixed at 0.015 m, while the roll motion was varied, with amplitudes of 1°, 3°, and 5°. The frequency of the coupled excitations was set to 1.0 ω_1'.

Fig. 9 shows the variations in sloshing pressure between the 16th and 21st cycles for Cases 1–6, together with the results for the pure sway scenario (amplitude: 0.015 m). It is seen that in Cases 1–3 (coupled excitations with the opposite-phase), the sloshing pressures are in-phase, thus causing higher pressures compared to those for pure sway. Moreover, as the amplitude of the roll excitation increases, sloshing pressure also increases due to the intensified sloshing-induced forces under the coupled sway-roll excitations. The variation in sloshing pressures becomes more unstable with an increase in the roll amplitude, leading to complex pressure variations. This phenomenon arises when the amplitude surpasses a specific threshold, resulting in roof impact. As the amplitude increases, in Cases 2 and 3, the impact on the roof intensifies, leading to significant deviations from linear predictions and the emergence of intricate pressure variations [26].

In Cases 4 and 5, it was observed that the sloshing pressures in the tank were decreased compared to those under pure sway. This reduction pressure results from the cancellation of sloshing-induced forces under coupled sway-roll excitations, primarily due to the phase alignment of the tank's excitation. This phase alignment occurs in the direction where the sloshing-induced forces generated in the tank by each sway and roll cancel each other out. In addition, the magnitude of the roll amplitude plays an important role in influencing this pressure decrease. In Case 4, with small roll amplitude of 1°, the pressure variations are mostly in phase with pure sway, but this results in a lower sloshing pressure compared to pure sway. In Case 5, however, the increased roll amplitude causes a deviation and shift in the phase of the pressure variation,

moving it out-of-phase, as shown in Fig. 9. A substantial phase shift occurred in Case 5 because the increased amplitude of the roll excitation influenced the sloshing motions more than the sway excitation. Case 5 exhibited the lowest sloshing pressures due to significant force cancellation, as indicated by the similarity between the average pressures for pure sway with an amplitude of 0.015 m and pure roll with an amplitude of 3° (see Table 2). Finally, Case 6 demonstrates that with a large roll amplitude of 5°, the roll excitation dominates the sloshing motion to the extent that the phase of pressure variations shifts to the opposite to that of pure sway, and also increases the pressure beyond the cancellation effect observed in Case 5.

Table 3 provides information on the maximum peak pressure during the initial 25s and the average values for the top 10% of sloshing pressures at point P_1 between the 16th and 21st cycles. Case 1 showed an increase of approximately 200 Pa in the maximum peak pressure compared to pure sway; although Cases 2 and 3 exhibited significantly higher maximum peak pressures compared to that of pure sway, the rise in the average pressures was not as significant as the increase in the maximum peak pressures. The dramatic increase in the maximum peak pressure (P_{max}) can be attributed to the instability of the pressure associated with the roof impact. In contrast, the maximum peak pressures and average pressures in both Cases 4 and 5 were lower than for pure sway. Case 6 showed higher pressures than for pure sway, as the cancellation of sloshing-induced forces was insignificant due to the unbalanced forces of the roll with a large amplitude of 5°, which imposed a phase shift toward the opposite of the sway motion.

The movements of the free surface of the liquid inside the tank under pure sway and in Cases 1–6 are presented in Fig. 10. It can be seen that under coupled sway-roll with the opposite-phase, the free surface flows became more complex with an increase in the amplitude of the roll. In contrast, when the sway and roll had the same-phase, sloshing did not exhibit significant oscillation compared to the opposite-phase cases (Cases 1–3). As a result, Case 5 (Fig 10(f)), with a roll amplitude of 3°, was the most stable, while Case 3 (Fig. 10(d)) exhibited the most unstable behaviour of the free surface.

Tab. 3. Maximum peak pressures and average pressures of the prismatic model tank for each scenario

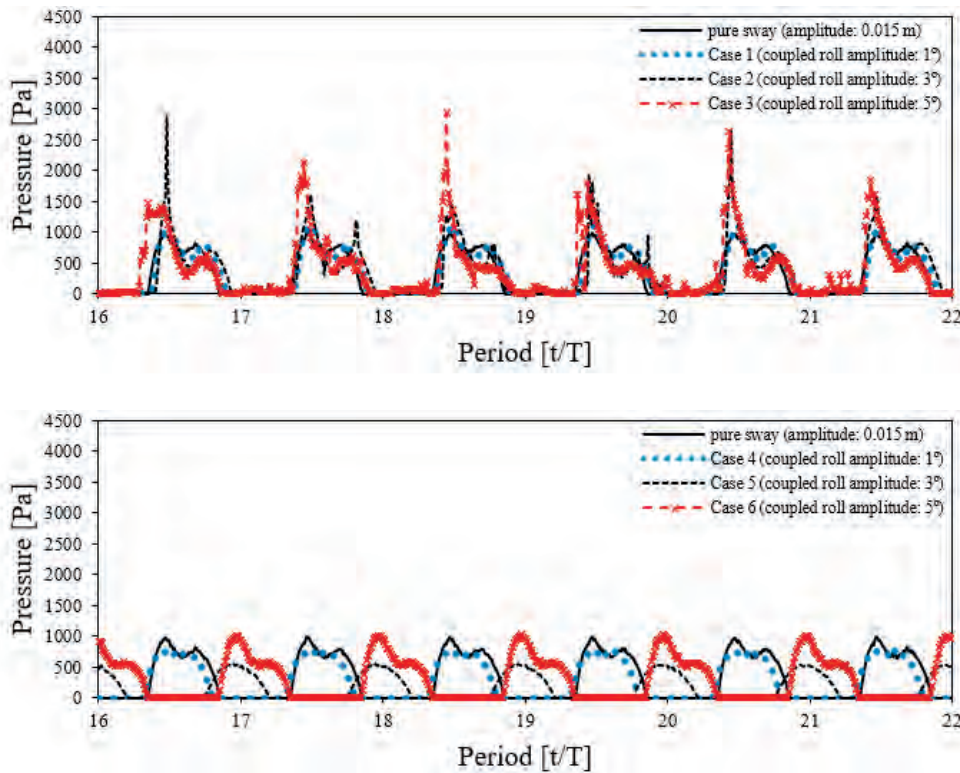| Scenario	P_{max} [Pa]	Time [s]	Average pressure [Pa]
Pure sway	1,037.687	9.55	903.424
Case 1	1,237.384	7.28	1,007.630
Case 2	3,277.842	6.17	1,342.786
Case 3	3,961.499	11.80	1,548.946
Case 4	800.638	16.35	749.527
Case 5	568.884	18.01	537.824
Case 6	1,179.679	7.83	953.605

Fig. 9. Comparison of pressure variations at P_1 of the prismatic model tank (over cycles 16 to 21): top graph (pure sway, Cases 1, 2, and 3) and bottom graph (pure sway, Cases 4, 5, and 6)
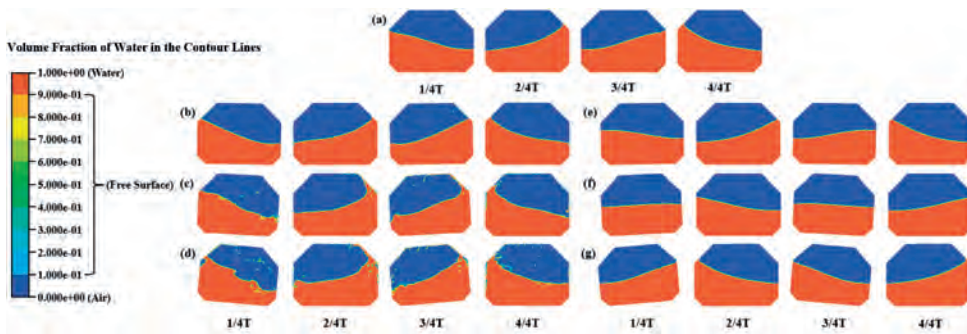

Fig. 10. Contours of the volume fraction of the prismatic model tank: (a) pure sway, (b) Case 1, (c) Case 2, (d) Case 3, (e) Case 4, (f) Case 5, (g) Case 6

FFT ANALYSIS

The sloshing pressure data obtained from 0–25 s were subjected to quantitative analysis using the FFT algorithm. This analysis focused on the time series data representing the sloshing pressures in the model tank under three scenarios: pure sway and coupled sway-roll excitations with both the same-phase and the opposite-phase. The results were examined in both the time domain and frequency domain, as shown in Fig. 11. Throughout the FFT analysis, we observed the presence of high-frequency noise exceeding 5 Hz in all

cases. To mitigate this noise, a filtering technique based on the FFT algorithm with a cutoff frequency of 5 Hz was employed [27].

In all cases, the analysis revealed that the highest amplitude of pressure occurred at the dominant frequency of the frequency domain, 0.88 Hz, which was closely approximated to the primary natural frequency of the tank, 1.0 ω'_1 (= 0.884918 Hz). Other pressure peaks were also observed at frequencies corresponding to integer multiples of the dominant frequency, specifically at 1.76, 2.64, 3.52, and 4.40 Hz. This observation suggests that in addition to the dominant frequency, these integer multiples of the dominant frequencies can also affect sloshing behaviour significantly [28]. The amplitudes of pressure at these frequencies are presented in Table 4, and pressure histories and FFT spectra are shown in Fig. 11.

In Case 1, the pressure amplitude at the dominant frequency was larger than that for pure sway, whereas in Cases 2 and 3, the amplitudes were very similar to that for pure sway. However, the amplitudes at frequencies of 1.76 and 2.64 Hz increased compared to those of both pure sway and Case 1. In Case 3, the amplitudes were larger in the vicinity of 3.52 and 4.40 Hz (i.e., 3.48, 3.56, 4.24, 4.36, 4.44, and 4.52 Hz), rather than at the 3.52 and 4.40 Hz. Furthermore, in Cases 2 and 3, sawtooth-shaped amplitude spectra were observed, implying the occurrence of complex sloshing phenomena. These phenomena were attributed to the nonlinear characteristics associated with irregular wave crests and breaking waves [29]. Fig. 11(c) and (d) demonstrate the instability of the sloshing pressure due to roof impacts, contributing to a significant increase in the pressure amplitude at or near the integer multiples of the dominant frequency (i.e., 1.76, 2.64, 3.52, and 4.40 Hz). In Cases 4–6, the pressure amplitudes at the dominant frequency were smaller than that for pure sway. This result is attributed to the cancellation effect between sloshing-induced forces due to coupled sway-roll excitations with the same-phase. In Case 5, the pressure amplitude at the dominant frequency was the smallest, as the largest cancellation occurred compared to the other cases.

These FFT results revealed several phenomena. Firstly, for coupled sway-roll with the opposite-phase without roof impact, the amplitudes of pressure increased at the dominant frequency compare to that of pure sway. Secondly, for coupled sway-roll having the opposite-phase with roof impact, the amplitudes of pressure resulted in tallest peaks that are similar in magnitudes and comparable to that of pure sway at the dominant frequency; while at or near integer multiples of the dominant frequency, most of the pressure peaks increased compare to that of pure sway. Thirdly, when the excitations are coupled with the same-phase, the amplitude at the dominant frequency decreased compare to the sway's. Finally, it was confirmed that the amplitude at the dominant frequency decreased significantly when the sloshing-induced forces of sway and roll, coupled in the same-phase, were similar.

Fig. 11. Pressure histories (with P_{max}) and FFT spectra at P_1 of the prismatic model tank: pure sway - (a) and (a´); Case 1 - (b) and (b´); Case 2 - (c) and (c´); Case 3 - (d) and (d´); Case 4 - (e) and (e´); Case 5 - (f) and (f´); and Case 6 - (g) and (g´)

Tab. 4. Amplitudes of sloshing pressure signals in the prismatic model tank at frequencies under different scenarios

Scenario	Frequency [Hz]				
	0.88	1.76	2.64	3.52	4.40
Pure sway	435.933	99.297	110.365	86.362	22.177
Case 1	447.610	83.227	156.256	95.055	31.253
Case 2	433.445	140.796	216.485	100.433	52.718
Case 3	437.104	212.115	179.821	50.733	29.098
Case 4	368.064	124.872	43.728	59.307	7.711
Case 5	216.485	98.965	8.619	21.374	6.767
Case 6	411.733	133.329	126.097	79.448	18.885

CONCLUSION

In this study, we investigated the liquid sloshing loads exerted on the inner walls of a KC-1 membrane LNG tank under various excitation scenarios. These scenarios included single excitations (pure sway and pure roll) and coupled sway-roll excitations, both with the same-phase and the opposite-phase, across different ranges of excitation amplitudes and frequencies. The findings revealed that the intensity of liquid sloshing loads significantly increases when the resonance effect occurs. Moreover, we observed that under coupled sway-roll excitations with the same-phase, the sloshing loads become weaker than that for the case of pure sway, except when the force of the roll is substantially larger than the force of the sway, such that it overcomes the diminishing effect. Conversely, when applied with the opposite-phase, coupled sway-roll excitations strengthen and increase the sloshing loads substantially more than in the case of pure sway.

FFT analysis further identified that when the excitation frequency was $1.0\ \omega_1'$, representing the first natural frequency of the tank, the sloshing pressure peaked predominantly at the dominant frequency, at 0.88 Hz, which is close to ω_1' (= 0.884918 Hz). Interestingly, under coupled sway-roll excitations with the same-phase, the amplitude of sloshing pressure at the dominant frequency was significantly reduced compared to that of pure sway, contrasting with the cases with the opposite-phase, where it was increased. When coupled sway-roll excitations were in the opposite-phase with no roof impact conditions, the amplitude at the dominant frequency increased. However, in the presence of roof impact during sloshing, instabilities in the free surface manifest, resulting in a nearly constant amplitude at the dominant frequency in comparison to the sway's. Concurrently, the amplitudes of sloshing at or in proximity to other integer multiples of the dominant frequency exhibit predominant increase.

This study has demonstrated that a resonance effect in the context of the sloshing phenomenon in a KC-1 tank occurs when the natural frequency of the fluid sloshing inside the tank aligns with the frequency of the external forces acting on the tank. This alignment can lead to significant amplification of the sloshing motion, potentially resulting in instability, the risk of fluid spillage, or even structural damage. In addition, when the overall time series data for sloshing pressure were analysed, instances of roof impact were
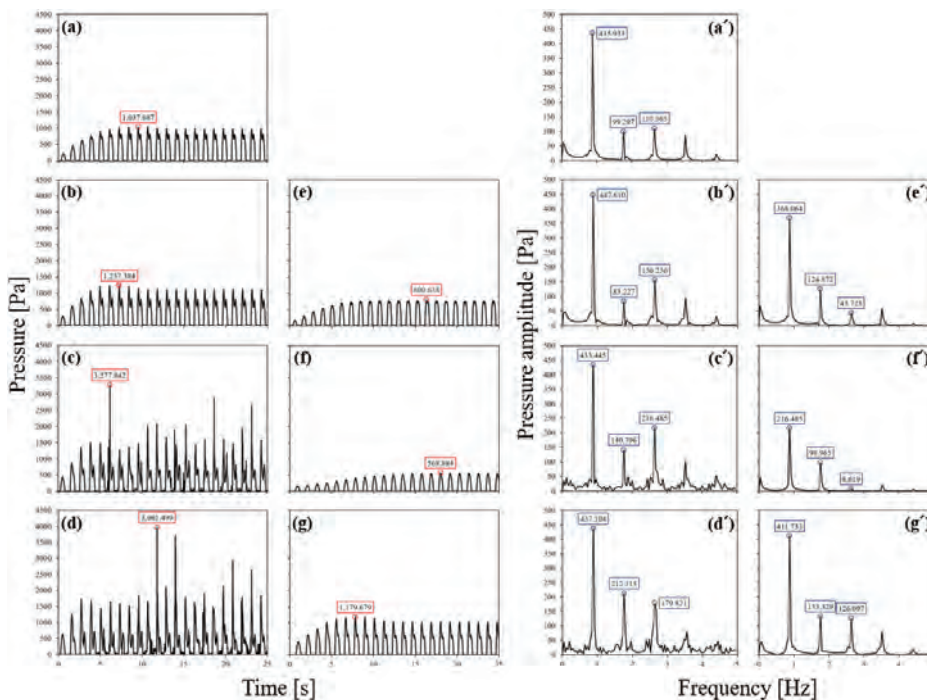
found to introduce instability into the pressure variations, making pressure predictions challenging. When the KC-1 tank is subjected to wave conditions involving both sway and roll excitation forces, there are measures that can be implemented to effectively mitigate the risk of substantial and unstable pressure surges. These measures include dampening or controlling the sloshing motion using baffles or dampers, promoting cancellation effects between the sloshing-induced forces stemming from each excitation, or adjusting the tank's natural frequency.

Further investigation will be necessary to explore the sloshing-induced forces in more diverse scenarios, including various types of multiple coupled excitations by manipulating the phases of the excitations with different filling heights. Moreover, it is important to expand the analysis domain from two dimensions to three, for a comprehensive understanding of the sloshing phenomenon.

ACKNOWLEDGEMENT

NOMENCLATURE

Denomination [units]

α	Volume fraction of liquid [-]
α_q	Volume fraction of phase q [-]
ρ	Density of the mixture [kg/m³]
ρ_q	Density of phase q [kg/m³]
$\vec{u}$	Velocity vector [m/s]
$\vec{u}_q$	Velocity vector of phase q [m/s]
S_{α_q}	Source term of phase q in a cell [kg/m³s]
$\dot{m}_{pq}$	Mass transfer from phase p to phase q [kg/m³s]
$\dot{m}_{qp}$	Mass transfer from phase q to phase p [kg/m³s]
p	Static pressure [N/m²]
$\overline{\overline{\tau}}$	Stress tensor [N/m²]
$\vec{g}$	Acceleration of gravity [m/s²]
$\vec{F}$	External body force [kg/m²s²]
μ	Dynamic viscosity [Pa s]
X	Horizontal displacement [m]
X_0	Amplitude of the sway excitation [m]
θ	Rotational displacement [°]
θ_0	Amplitude of the roll excitation [°]
ω	Frequency [rad s⁻¹]
t	Time [s]
H	Total height [m]
H_1	Height of the chamfered bottom corner [m]
H_2	Height excluding the corners [m]
H_3	Height of the chamfered upper corner [m]
B	Total breadth [m]
B_1	Breadth of the chamfered bottom corner [m]
B_2	Breadth of the chamfered upper corner [m]
θ_1	Angle of the chamfered upper corner [°]
θ_2	Angle of the chamfered bottom corner [°]
h	Height of the water filling [m]
ω_1	First natural frequency of the rectangular tank [rad s⁻¹]
ω_1'	First natural frequency of the prismatic tank [rad s⁻¹]
P_1	Internal pressure point in the rectangular tank and prismatic tank [Pa]
P_{max}	Maximum peak pressure [Pa]

REFERENCES

1. H. N. Abramson, "The dynamic behavior of liquids in moving containers, with applications to space vehicle technology," Department of Mechanical Sciences, Southwest Research Institute, Washington, D.C., NASA-SP-106, 1966.

2. L. Hou, F. Li, and C. Wu, "A numerical study of liquid sloshing in a two-dimensional tank under external excitations," *Journal of Marine Science and Application*, vol. 11, pp. 305-310, September 2012, doi: 10.1007/s11804-012-1137-y.

3. B. F. Chen and C. H. Wu, "Effects of excitation angle and coupled heave-surge-sway motion on fluid sloshing in a three-dimensional tank," *Journal of Marine Science and Technology*, vol. 16, pp. 22-50, December 2011, doi: 10.1007/s00773-010-0111-0.

4. W. Wu, C. Zhen, J. Lu, J. Tu, J. Zhang, Y. Yang, K. Zhu, and J. Duan, "Experimental study on characteristic of sloshing impact load in elastic tank with low and partial filling under rolling coupled pitching," *International Journal of Naval Architecture and Ocean Engineering*, vol. 12, pp. 178-183, 2020, doi: 10.1016/j.ijnaoe.2019.10.003.

5. B. Godderidge, S. R. Turnock, and M. Tan, "Evaluation of a rapid method for the simulation of sloshing in rectangular and octagonal containers at intermediate filling levels," *Computers & Fluids*, vol. 57, pp. 1-24, March 2012, doi: 10.1016/j.compfluid.2011.09.010.

6. H. Jeong and W. Jaewoo Shim, "Calculation of boil-off gas (BOG) generation of KC-1 membrane LNG tank with high density rigid polyurethane foam by numerical analysis," *Polish Maritime Research*, vol. 24, no. 1, pp. 100-114, April 2017, doi: 10.1515/pomr-2017-0012.

7. C. W. Hirt and B. D. Nichols, "Volume of fluid (VOF) method for the dynamics of free boundaries," *Journal of Computational Physics*, vol. 39, no. 1, pp. 201-225, January 1981, doi: 10.1016/0021-9991(81)90145-5.

8. J. Haider, "Numerical modelling of evaporation and condensation phenomena," Thesis, Institut für Raumfahrtsysteme, Universität Stuttgart, Lampoldshausen, 2013.

9. V. Singal, J. Bajaj, N. Awalgaonkar, and S. Tibdewal, "CFD analysis of a kerosene fuel tank to reduce liquid sloshing," *Procedia Engineering*, vol. 69, pp. 1365-1371, 2014, doi: 10.1016/j.proeng.2014.03.130.

10. A. B. Desamala, V. Vijayan, A. Dasari, A. K. Dasmahapatra, and T. K. Mandal, "Prediction of oil-water flow patterns, radial distribution of volume fraction, pressure and velocity during separated flows in horizontal pipe," *Journal of Hydrodynamics*, vol. 28, pp. 658-668, August 2016, doi: 10.1016/S1001-6058(16)60670-4.

11. M. L. Hosain, U. Sand, R. Bel Fdhila, "Numerical investigation of liquid sloshing in carrier ship fuel tanks," *IFAC-PapersOnLine*, vol. 51, no. 2, pp. 583-588, 2018, doi: 10.1016/j.ifacol.2018.03.098.

12. S. H. Rhee, "Unstructured grid based Reynolds-averaged Navier-Stokes method for liquid tank sloshing," *Journal of Fluids Engineering*, vol. 127, no. 3, pp. 572-582, 2005, doi: 10.1115/1.1906267.

13. O. M. Faltinsen and A. N. Timokha, "An adaptive multimodal approach to nonlinear sloshing in a rectangular tank," *Journal of Fluid Mechanics*, vol. 432, pp. 167-200, April 2001, doi: 10.1017/S0022112000003311.

14. O. M. Faltinsen and A. N. Timokha, "Analytically approximate natural sloshing modes and frequencies in two-dimensional tanks," *European Journal of Mechanics – B/Fluids*, vol. 47, pp. 176-187, September-October 2014, doi: 10.1016/j.euromechflu.2014.01.005.

15. N. Parthasarathty, H. Kim, Y. H. Choi, and Y. W. Lee, "A numerical study on sloshing impact loads in prismatic tanks under forced horizontal motion," *Journal of the Korean Society of Marine Engineering*, vol. 41, no. 2, pp. 150-155, 2017, doi: 10.5916/jkosme.2017.41.2.150.

16. M. Hinatsu, "Experiments of two-phase flows for the joint research," In: Proceedings of the SRI-TUHH mini-Workshop on Numerical Simulation of Two-Phase Flows, Ship Research Institute, Tokyo, Japan, pp. 12-19, 2001.

17. Y. H. Chen, Y. F. Yue, Y. Zhang, R. P. Li, and X. Xu, "Numerical investigation of vibration suppression for the combined device of non-Newtonian fluids coupled elastic baffle," *Journal of Applied Fluid Mechanics*, vol. 16, no. 3, pp. 591-602, 2023, doi: 10.47176/jafm.16.03.1311.

18. H. Jin, Y. Liu, H. Li, and Q. Fu, "Numerical analysis of the flow field in a sloshing tank with a horizontal perforated plate," *Journal of Ocean University of China*, vol. 16, no. 4, pp. 575-584, 2017, doi: 10.1007/s11802-017-3369-6.

19. O. Ubbink, "Numerical prediction of two fluid systems with sharp interfaces," Thesis, Department of Mechanical Engineering, London University, January 1997.

20. B. Godderidge, S. Turnock, C. Earl, and M. Tan, "The effect of fluid compressibility on the simulation of sloshing impacts," *Ocean Engineering*, vol. 36, no. 8, pp. 578-587, June 2009, doi: 10.1016/j.oceaneng.2009.02.004.

21. C. Hu and M. M. Kamra, "An unstructured mesh method for numerical simulation of violent sloshing flows," *Journal of Hydrodynamics*, vol. 32, no. 2, pp. 259-266, April 2020, doi: 10.1007/s42241-020-0019-z.

22. B. Godderidge, S. Turnock, M. Tan, and C. Earl, "An investigation of multiphase CFD modelling of a lateral sloshing tank," *Computers & Fluids*, vol. 38, no. 2, pp. 183-193, February 2009, doi: 10.1016/j.compfluid.2007.11.007.

23. H. Akyildiz and E. Ünal, "Experimental investigation of pressure distribution on a rectangular tank due to the liquid sloshing," *Ocean Engineering*, vol. 32, no. 11-12, pp. 1503-1516, 2005, doi: 10.1016/j.oceaneng.2004.11.006.

24. J. H. Jung, H. S. Yoon, and C. Y. Lee, "Effect of natural frequency modes on sloshing phenomenon in a rectangular tank," *International Journal of Naval Architecture and Ocean Engineering*, vol. 7, no. 3, pp. 580-594, May 2015, doi: 10.1515/ijnaoe-2015-0041.

25. S. Wu and Y. Ju, "Numerical study of the boil-off gas (BOG) generation characteristics in a type C independent liquefied natural gas (LNG) tank under sloshing excitation," *Energy*, vol. 223, no. 15, pp. 1-19, May 2021, doi: 10.1016/j.energy.2021.120001.

26. K. P. Thiagarajan, D. Rakshit, and N. Repalle, "The air-water sloshing problem: Fundamental analysis and parametric studies on excitation and fill levels," *Ocean Engineering*, vol. 38, no. 2-3, pp. 498-508, 2011, doi: 10.1016/j.oceaneng.2010.11.019.

27. H. Kim, P. Nanjundan, J. Jeon, and Y. W. Lee, "Numerical estimation on applying air-trapping mechanism to suppress sloshing loads in a prismatic tank," *Journal of Mechanical Science and Technology*, vol. 34, no. 7, pp. 2895-2902, 2020, doi: 10.1007/s12206-020-0621-6.

28. X. Yuan, Y. Su, and P. Xie, "Frequency characteristics of sloshing resonance in a three-dimensional shallow-water rectangular tank," *Journal of Marine Science and Engineering*, vol. 10, no. 11, pp. 1792-1804, November 2022, doi: 10.3390/jmse10111792.

29. H. Kim, M. K. Dey, N. Oshima, and Y. W. Lee, "Numerical study on sloshing characteristics with Reynolds number variation in a rectangular tank," *Computation*, vol. 6, no. 4, pp. 53-63, October 2018, doi: 10.3390/computation6040053.